J|A|C|S
ARTICLES

Published on Web 03/10/2009

Single-Chromophore-Based Photoswitchable Nanoparticles Enable Dual-Alternating-Color Fluorescence for Unambiguous Live Cell Imaging

Zhiyuan Tian, Wuwei Wu, Wei Wan, and Alexander D. Q. Li*

Department of Chemistry and Center for Materials Research, Washington State University, Pullman, Washington 99164

Received July 3, 2008; E-mail: dequan@wsu.edu

Abstract: We have developed a class of spiropyran dyes and their fluorescence colors can be reversibly photoswitched from red to green, blue, or nearly dark, thus alternating between two colors. Such individual dyes emit either one color or the other but not both simultaneously. Nanoparticles enabled with these photoswitchable dyes, however, emit either one pure color or a combination of both colors because the nanoparticle fluorescence originates from multiple dyes therein. As a result, the nanoparticle shines >30 times brighter than state-of-the-art organic dyes such as fluorescein. Interestingly, these copolymer nanoparticles exhibit tunable nonspecific interactions with live cells, and nanoparticles containing properly balanced butyl acrylate and acrylamide monomers render essentially very little nonspecific binding to live cells. Decorated with HMGA1 protein, these optically switchable dual-color nanoparticles undergo endocytosis and unambiguously identify themselves from fluorescence interference including autofluorescence, thus enabling a new tool for live cell imaging.

Introduction

Live cell optical imaging has provided a wealth of information regarding biological mechanisms and dramatically transformed biological sciences in the past few decades.[1−14] The key enabling technology is the fluorescent probe. Ultimately, fluorescent imaging demands brighter probes to detect and monitor individual molecular events, smarter surface coating on probes to reduce nonspecific interactions with biological systems, and photoswitchable molecules to achieve multicolor high-resolution imaging.

Brighter probes require large extinction coefficients and high quantum yields. Because current fluorescent dyes already have efficient quantum yields (ca. 50−90%) approaching the theoretical limit of unity, efforts to enhance this feature are unlikely to dramatically increase the brightness. Therefore, the alternative solution to ultrabright probes is to increase the molar extinction coefficient without sacrificing the quantum yield. Both quantum dots and dye-embedded nanospheres had capitalized on large molar extinction coefficients and produced much brighter probes for biomedical imaging.[9,10,15] Typically, they are 10−30 times brighter than the most fluorescent organic dyes.[1−8,16−19] Additionally, quantum dots and dye-embedded nanoparticles benefit from more resistance to photobleaching, and this characteristic feature allows relatively long-term monitoring or tracking of the same tagged biological cargoes such as endosomes.

Another desired property for biological imaging requires the fluorescent probes not to interact nonspecifically with nontargeted cells or tissue.[20] The most severe undesired interactions

(1) Bruchez, M.; Moronne, M.; Gin, P.; Weiss, P.; Alivisatos, A. P. *Science* **1998**, *281*, 2013–2016.
(2) Chan, W. C. W.; Nie, S. M. *Science* **1998**, *281*, 2016–2018.
(3) Chan, W. C. W.; Maxwell, D. J.; Gao, X. H.; Bailey, R. E.; Han, M. Y.; Nie, S. M. *Curr. Opin. Biotechnol.* **2002**, *13*, 40–46.
(4) Dubertret, B.; Skourides, P.; Norris, D. J.; Noireaux, V.; Brivanlou, A. H.; Libchaber, A. *Science* **2002**, *298*, 1759–1762.
(5) Akerman, M. E.; Chan, W. C. W.; Laakkonen, P.; Bhatia, S. N.; Ruoslahti, E. *Proc. Natl. Acad. Sci. U.S.A.* **2002**, *99*, 12617–12621.
(6) Wu, X. Y.; Liu, H. J.; Liu, J. Q.; Haley, K. N.; Treadway, J. A.; Larson, J. P.; Ge, N. F.; Peale, F.; Bruchez, M. P. *Nat. Biotechnol.* **2003**, *21*, 41–46.
(7) Jaiswal, J. K.; Mattoussi, H.; Mauro, J. M.; Simon, S. M. *Nat. Biotechnol.* **2003**, *21*, 47–51.
(8) Larson, D. R.; Zipfel, W. R.; Williams, R. M.; Clark, S. W.; Bruchez, M. P.; Wise, F. W.; Webb, W. W. *Science* **2003**, *300*, 1434–1436.
(9) Santra, S.; Xu, J. S.; Wang, K. M.; Tan, W. H. *J. Nanosci. Nanotechnol.* **2004**, *4*, 590–599.
(10) Buck, S. M.; Xu, H.; Brasuel, M.; Philbert, M. A.; Kopelman, R. *Talanta* **2004**, *63*, 41–59.
(11) Michalet, X.; Pinaud, F. F.; Bentolila, L. A.; Tsay, J. M.; Doose, S.; Li, J. J.; Sundaresan, G.; Wu, A. M.; Gambhir, S. S.; Weiss, S. *Science* **2005**, *307*, 538–544.
(12) Howarth, M.; Takao, K.; Hayashi, Y.; Ting, A. Y. *Proc. Natl. Acad. Sci. U.S.A.* **2005**, *102*, 7583–7588.
(13) Cao, Z. H.; Huang, C. C.; Tan, W. H. *Anal. Chem.* **2006**, *78*, 1478–1484.
(14) Liu, W.; Howarth, M.; Greytak, A. B.; Zheng, Y.; Nocera, D. G.; Ting, A. Y.; Bawendi, M. G. *J. Am. Chem. Soc.* **2008**, *130*, 1274–1284.
(15) Rosen, A. B.; Kelly, D. J.; Schuldt, A. J. T.; Lu, J.; Potapova, I. A.; Doronin, S. V.; Robichaud, K. J.; Robinson, R. B.; Rosen, M. R.; Brink, P. R.; Gaudette, G. R.; Cohen, I. S. *Stem Cells* **2007**, *25*, 2128–2138.
(16) Mattoussi, H.; Mauro, J. M.; Goldman, E. R.; Anderson, G. P.; Sundar, V. C.; Mikulec, F. V.; Bawendi, M. G. *J. Am. Chem. Soc.* **2000**, *122*, 12142–50.
(17) Ishii, D.; Kinbara, K.; Ishida, Y.; Ishii, N.; Okochi, M.; Yohda, M.; Aida, T. *Nature* **2003**, *423*, 628–632.
(18) Medintz, I. L.; Clapp, A. R.; Mattoussi, H.; Goldman, E. R.; Fisher, B.; Mauro, J. M. *Nat. Mater.* **2003**, *2*, 630–638.
(19) Dahan, M.; Levi, S.; Luccardini, C.; Rostaing, P.; Riveau, B.; Triller, A. *Science* **2003**, *302*, 442–445.
(20) Chen, A. K.; Behlke, M. K.; Tsourkas, A. *Nucleic Acids Res.* **2007**, *35*, e105/1−12.

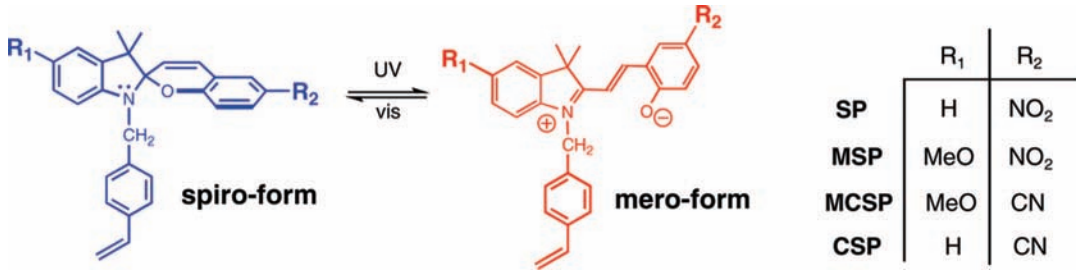

Figure 1. Chemical structures illustrate the spiro and mero forms of the photoswitchable fluorescent dyes and how photochemical reactions switch red fluorescence to dark state (SP), green fluorescence (MSP), and blue fluorescence (MCSP and CSP).

result in toxicities to biological systems, while others include labeling the nontargeted cells or tissue, generating false positives. Therefore, although tremendous progress has been made to target specific cell types by use of highly selective protein−protein interactions such as antibody−antigen binding, relatively little research is devoted to minimize nonspecific interactions. Obviously both are important. An ideal probe should maximize its specific interactions to the targeted proteins, cells, or tissue while minimizing its nonspecific interactions with surrounding biological materials. To this end, we have discovered that synthetic copolymers and their composition and sequences greatly affect nonspecific interactions. These copolymers can offer new protecting shells for fluorescent probes such as polymer nanoparticles and quantum dots to further reduce nonspecific interactions.

Brighter probes enable imaging individual molecular events and phenomena, but fluorescence switching such as fluorescence resonance energy transfer (FRET) has revolutionized biological studies of molecular interactions. FRET requires two fluorescent dyes: one (the fluorescent donor) emits high-energy photons and the other (the fluorescent acceptor) emits low-energy photons.[21−24] When the donor and acceptor approach each other near or within the Förster distance, fluorescence color switches from the donor to the acceptor, or from high- to low-energy photons. Pairs of fluorescent dyes such as Cy3 and Cy5, when properly positioned, also exhibit optical switching phenomena; such on−off fluorescence switching has enabled new high-resolution imaging techniques such as stochastic optical reconstruction microscope (STORM).[25−27] If a single dye can carry out fluorescence switching, offering either fluorescence on-and-off or fluorescence color change, it greatly simplifies sample labeling and eliminates the necessary procedures to integrate two dyes into the required situation. Such wonderful dyes appear be implausible. Recently, however, we have demonstrated these unthinkable dyes in spiropyran derivatives. One molecule alternately emits two distinct fluorescence colors. Amazingly, photoexcitation can switch one fluorescence color to the other and vice versa. The fluorescence on-and-off or fluorescence color switching possesses digital on-and-off quality and enables "communication" between the investigator and the probe, thus unambiguously identifying the switchable probes.

Herein, we use such photoswitchable molecules to fabricate nanoparticles, whose fluorescence color can be optically switched either from one color to another or on-and-off. Because multiple dyes reside in a single particle, the resulting nanoparticle fluorescence is at least 30 times brighter than organic dyes. Tuning the copolymer composition and sequences effectively reduces the nanoparticle nonspecific interactions with cell membranes. Such feature-packed nanoparticles will further advance biomedical imaging capabilities, and here we will report their construction, spectroscopic characterization, and initial live cell imaging results.

Results and Discussion

Single-Dye-Enabled Dual-Color Fluorescence Photoswitching in Nanoparticles: Synthesis and Characterization. The polymer nanoparticles investigated here were constructed following previous literature procedures to incorporate various photochromic spiropyran derivatives into the hydrophobic cores of the nanoparticles.[28−30] Typically, major monomers acrylamide (A), styrene (ST), and butyl acrylate (BA) were polymerized with minor functional monomers, including optically switchable spiropyran derivatives, the cross-linker divinylbenzene (DVB), and water-soluble acrylic acid (AA) decorating the nanoparticle surfaces. The nanoparticles used in this paper range from 60 to 80 nm as characterized by transmission electron microscopy (TEM) and light scattering unless otherwise stated. Light scattering revealed no particle aggregation in solution. Previously dual-color photoswitching was achieved by FRET between two dyes: one photochromic spiropyran and another fluorescence donor chromophore. Now, a single spiropyran derivative molecule enables dual-color photoswitching in nanoparticles.

Figure 1 illustrates four spiropyran derivatives investigated: 3′,3′-dimethyl-6-nitro-1′-(4-vinylbenzyl)spiro[chromene-2,2′-indoline] (SP); 5′-methoxy-3′,3′-dimethyl-6-nitro-1′-(4-vinylbenzyl)spiro[chromene-2,2′-indoline] (MSP); 5′-methoxy-3′,3′-dimethyl-6-cyano-1′-(4-vinylbenzyl)spiro[chromene-2,2′-indoline] (MCSP); and 3′,3′-dimethyl-6-cyano-1′-(4-vinylbenzyl)spiro[chromene-2,2′-indoline] (CSP). The nanoparticles containing SP exhibit fluorescence on-and-off switching properties between red fluorescence and dark state. When the photo-

(21) Stryer, L.; Haugland, R. P. *Proc. Natl. Acad. Sci. U.S.A.* **1967**, *58*, 719–726.
(22) Ha, T.; Enderle, Th.; Ogletree, D. F.; Chemla, D. S.; Selvin, P. R.; Weiss, S. *Proc. Natl. Acad. Sci. U.S.A.* **1996**, *93*, 6264–6268.
(23) Ha, T.; Zhuang, X. W.; Kim, H. D.; Orr, J. W.; Williamson, J. R.; Chu, S. *Proc. Natl. Acad. Sci. U.S.A.* **1999**, *96*, 9077–9082.
(24) Giepmans, B. N. G.; Adams, S. R.; Ellisman, M. H.; Tsien, R. Y. *Science* **2006**, *312*, 217–224.
(25) Rust, M. J.; Bates, M.; Zhuang, X. W. *Nat. Methods* **2006**, *3*, 793–796.
(26) Bates, M.; Huang, B.; Dempsey, G. T.; Zhuang, X. W. *Science* **2007**, *317*, 1749–1753.
(27) Huang, B.; Wang, W.; Bates, M.; Zhuang, X. W. *Science* **2008**, *319*, 810–813.
(28) Chen, M.-Q.; Kishida, A.; Akashi, M. *J. Polym. Sci., Part A: Polym. Chem.* **1996**, *34*, 2213–2220.
(29) Ishizu, K.; Yamashita, M.; Ichimura, A. *Polymer* **1997**, *38*, 5471–5474.
(30) Zhu, M. Q.; Zhu, L. Y.; Han, J. J.; Wu, W. W.; Hurst, J. K.; Li, A. D. Q. *J. Am. Chem. Soc.* **2006**, *128*, 4303–4309.

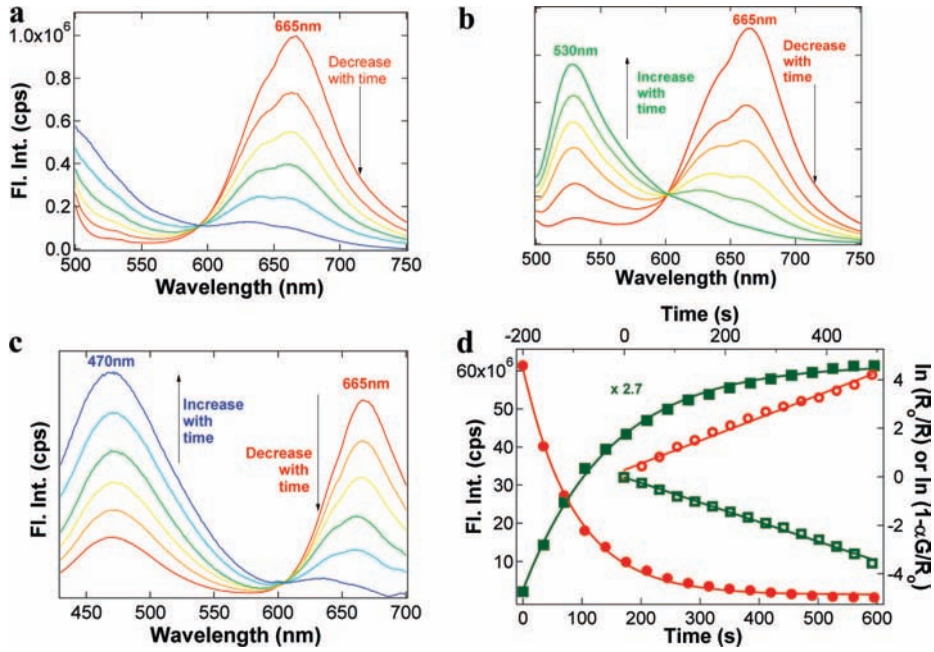

Figure 2. (a) After UV irradiation (365 nm), 1.5 nM 62-nm SP-nanoparticles containing the mero-form dyes were excited at 488 nm and photoswitched back to the "dark" state (spiro form). (b) The 365-nm illumination switched the 61-nm MSP-nanoparticles to the red fluorescence state, and subsequently fluorescence switching was monitored when the sample was excited at 488 nm. (c) MCSP residing in 71-nm nanoparticles was photoswitched to the mero form by use of 300-nm illumination; then the nanoparticle fluorescence was measured by use of 365-nm illumination to excite their 1.5 nM solution. (d) When red-fluorescing nanoparticles were photoswitched to green-emitting nanoparticles, integrated fluorescence peak areas reveal monoexponential evolution (solid symbols; left and bottom axes). The red-fluorescence decay (red open circles) yields a kinetic rate of 0.0079 ± 0.0005 s^{-1}, which agrees with the green-fluorescence growth kinetic rate of 0.007 ± 0.0009 s^{-1} (top and right axes). The factor $\alpha = 2.7$ is defined as the mero-to-spiro fluorescence integrated-intensity ratio when the mero-form concentration equals the spiro-form concentration, [mero] = [spiro].

switchable SP is in its ring-closed spiro form, it hardly fluoresces. However, UV-induced ring opening converts the spiro form to merocyanine or mero form,[31] which absorbs strongly at λ_{max} ~570 nm and fluoresces strongly at λ_{max} ~665 nm when the mero dyes reside in polymeric nanoparticles. Thus, nanoparticles containing SP (SP-nanoparticles) can be photoswitched between high-quantum-yield red fluorescence and dark state.[30] Similarly, MCSP and MSP also undergo photoinduced ring-opening reaction, but instead of producing on-and-off fluorescence they switch the fluorescence color. The MCSP-nanoparticles and CSP-nanoparticles containing MCSP and CSP, respectively, possess blue (470 nm) to red (665 nm) fluorescence color switching. The nanoparticles containing MSP (MSP-nanoparticles) switch between green (530 nm) and red (665 nm) fluorescence. The color-switching nanoparticles emit either one of the two pure colors or any color from the two-color combination. The photostability of such switchable dyes has been reported, and their photobleaching times were similar to other efficient dyes.[32]

Figure 2a−c displays one complete half-cycle in which red-fluorescing nanoparticles are photoswitched to dark state or green or blue fluorescence. For a single spiropyran molecule, a low-power UV pulse will instantaneously switch on the red fluorescence. For spiropyran-functionalized nanoparticles, we typically use a 3-mW/cm^2 UV lamp for 3 s duration to switch from blue to red fluorescence. Importantly, Figure 2b demonstrates pure red color is switched to pure green color. The fluorescence intensity ratio defines the color purity. In the red-fluorescence state, the fluorescence color is considered red if the red/green fluorescence intensity quotient exceeds $r_{R/G} = 10$. Conversely, this same ratio drops below $r_{R/G} = 0.1$ in the green-fluorescence state. Thus, the fluorescence intensity ratio alters by 100 times in a complete photoswitching half-cycle. Informatively, all fluorescence spectra in Figure 2a−c reveal an isosbestic fluorescence point, suggesting a clean one-to-one photochemical conversion.

The red-to-green fluorescence switching or mero to spiro form also occurs thermally, but photoexciting merocyanine absorption greatly accelerates the kinetics. Every 100 s, we pulsed the merocyanine for 3 s and obtained the "thermally" driven mero-to-spiro chemical conversion, $k_{th} = 1.6 \times 10^{-2}$ min^{-1} with a half-time $t_{1/2}^{th} = 43$ min. Similarly, but exciting the sample constantly with 488-nm light, we measured the photochemically stimulated mero-to-spiro kinetics, yielding $k_{all} = (7.9 \pm 0.5) \times 10^{-3}$ s^{-1} with half-time $t_{1/2}^{all} = 1.46$ min (Figure 2d) and accelerating the reaction by ~30 times. The photochemically accelerated process includes both thermal and photochemical contribution to the mero-to-spiro conversion, thus $k_{all} = k_{th} + k_{h\nu}$. As a result, a pure hypothetical photochemical conversion has a half-time $t_{1/2}^{h\nu} = 1.5$ min, slightly slower than the half-time when both effects are driving the reaction. These kinetic constants involving photoirradiation depend on many factors such as light wavelength and intensity as well as solution concentration because the effective light-penetration depth and optical absorption determine the rate of the photochemical reaction.

If one mero molecule is photochemically converted to one spiro molecule, then the properly scaled fluorescence intensities should mirror each other: one decreases while the other increases proportionally. Figure 2d plots both red- and green-fluorescence trends as time elapses, and indeed the green fluorescence gains

(31) Menju, A.; Hayashi, K.; Irie, M. *Macromolecules* **1981**, *14*, 755–758.
(32) Hu, D. H.; Tian, Z. Y.; Wu, W. W.; Wan, W.; Li, A. D. Q. *J. Am. Chem. Soc.* **2008**, *130*, 15279–15281.

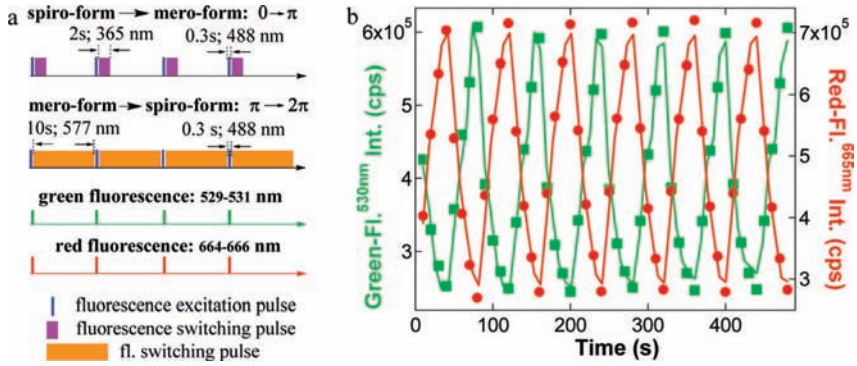

Figure 3. (a) Pulse sequences that elicited the dual-fluorescence color switching used three colors. The forward switching, from spiro to mero, used four 365-nm UV pulses at 2-s duration, followed by an 8-s delay before fluorescence was measured by use of 488-nm illumination for 0.3 s duration. The backward switching, from mero to spiro, used four wide 10-s pulses at the mero absorption band, 577 nm, while fluorescence was measured without delay by use of 488-nm excitation right after each switching pulses. (b) The pulse sequences in panel a generate red- and green-fluorescence oscillation. The nearly antiphase-synchronized red and green fluorescence were measured at 665 and 530 nm, respectively. Symbols represent data, and modulation fitting yields oscillation frequency and phase difference up to the fourth harmonic.

at the expense of the red fluorescence. Red fluorescence exponentially decreases while green fluorescence exponentially increases. Both follow first-order kinetics. The disappearing spiro form proceeds with rate constant $k_{all}^{red} = (7.9 \pm 0.5) \times 10^{-3}$ s^{-1}, but the emerging mero form occurs at a slightly slower rate constant, $k_{all}^{green} = (7.0 \pm 0.9) \times 10^{-3}$ s^{-1} (Figure 2d). The fact that $k_{all}^{red} \approx k_{all}^{green}$ indicates that mero-to-spiro photochemical reaction occurs nearly simultaneously or with extremely short-lived intermediates. The spiro-to-mero conversion reacts immediately and therefore the mero-to-spiro photochemical process becomes the rate-determining step and controls the fluorescence modulation cycles and frequency.

Exciting MSP-nanoparticles at 365 nm causes the spiro bond to rupture and the MSP structure changes to its corresponding merocyanine dye, which has extended π-conjugation terminated by electron donor and acceptor, thus emitting red fluorescence. Conversely, pumping photons into the merocyanine absorption (577 nm) drives the reaction back, re-forming the spiro bond and recovering the MSP structure, which has less extensive conjugation and therefore fluoresces green color. Thus, alternating 365- and 577-nm photoexcitation results in undulating red and green fluorescence in nearly antiphase synchronization (Figure 3a). To further understand the relationship between red and green fluorescence synchronization, we plot fluorescence oscillation against time in Figure 3b and fit the modulated fluorescence intensity to a series of periodic functions up to the fourth harmonic:

$$G = G_0 + G_1 \sin(\omega_G t + \varphi_{G1}) + G_2 \sin^2(\omega_G t + \varphi_{G2}) + G_3 \sin^3(\omega_G t + \varphi_{G3}) + \ldots$$

$$R = R_0 + R_1 \sin(\omega_R t + \varphi_{R1}) + G_2 \sin^2(\omega_R t + \varphi_{R2}) + G_3 \sin^3(\omega_R t + \varphi_{R3}) + \ldots$$

where G and R represent green and red fluorescence intensity; G_0 and R_0 are the DC components of green and red fluorescence intensity; and G_1, G_2, G_3,..., and R_1, R_2, R_3,..., etc., are modulation amplitude at the fundamental (ω) or high harmonic frequencies (2ω, 3ω,...), respectively. Modeling reveals that red and green fluorescence synchronize at $\omega_R = \omega_G = 0.0786$ s^{-1} or 12.5 mHz and oscillate almost completely out of phase, $\Delta\phi_1 = \phi_{R1} - \phi_{G1} = 176° \pm 2°$. The frequency matching ($\omega_R = \omega_G$) suggests that an intrinsic relationship locks the green and red fluorescence undulation and that relationship reflects the one-to-one spiro−mero photochemical conversion. The nearly antiphase synchronization reflects that red fluorescence peaks at its maximum slightly before green fluorescence will reach the minimum. The almost ~180° phase shift also suggests that the green fluorescence synchronizes with the red fluorescence, indicating the spiro and mero form forward and backward interconversion occurs nearly simultaneously or with extremely short-lived intermediates. These results agree with the kinetics studies.

The ability to modulate fluorescence intrinsically enables a new fluorescence detection technique. Because only photoswitchable dyes or nanoparticles are responding to the photoswitching pulses, the modulated fluorescence emission has a distinct frequency for the observer to lock on, thus eliminating the zero-frequency fluorescence noise from the desired signal oscillating at ω. Using lock-in technology, one can detect fluorescence from spiropyran dyes or spiropyran-based FRET pairs more sensitively by using the known modulation frequency.

Nanoparticles Glow Much Brighter Than Organic Dyes. Nanoparticles offer the desired fluorescence brightness. Although unprotected MSP dyes have a low quantum yield, MSP molecules residing in the hydrophobic core of nanoparticles acquire a good quantum yield of $\Phi = 0.28$ for red fluorescence when compared to rhodamine B.[30] Figure 4 reveals the brightness of the dual-color nanoparticles and fluorescein dye. At such an excitation power, fluorescein individual molecules (right) emit on-average 180 counts per second (cps), just above dark counts (~50), whereas the singly isolated nanoparticles are shining much brighter, emitting 2500 cps (Figure 4a). Figure 4b is plotted using the exact color scale of the nanoparticles, and this color scale blinds fluorescein emission completely. To reveal individual fluorescein emitters, we plot the fluorescein dye image at a much lower brightness scale and the individual molecular emitters finally emerge as shining spots (Figure 4c).

Figure 4d displays the statistic brightness occurrence against the brightness to generate a histogram that reveals the brightness difference between nanoparticles and fluorescein molecules. To accommodate the dramatic brightness disparity, the horizontal axis is plotted logarithmically. The histogram demonstrates that a typical nanoparticle glows ~14 times brighter than a single fluorescein dye. Although both the nanoparticle and the fluorescein dye were calibrated under exactly the same experimental conditions, the excitation wavelength matches the fluorescein absorption band at 488 nm, at which wavelength, however, neither the spiro nor the mero dye absorbs appreciably. When the excitation wavelength moves from 488 nm to the

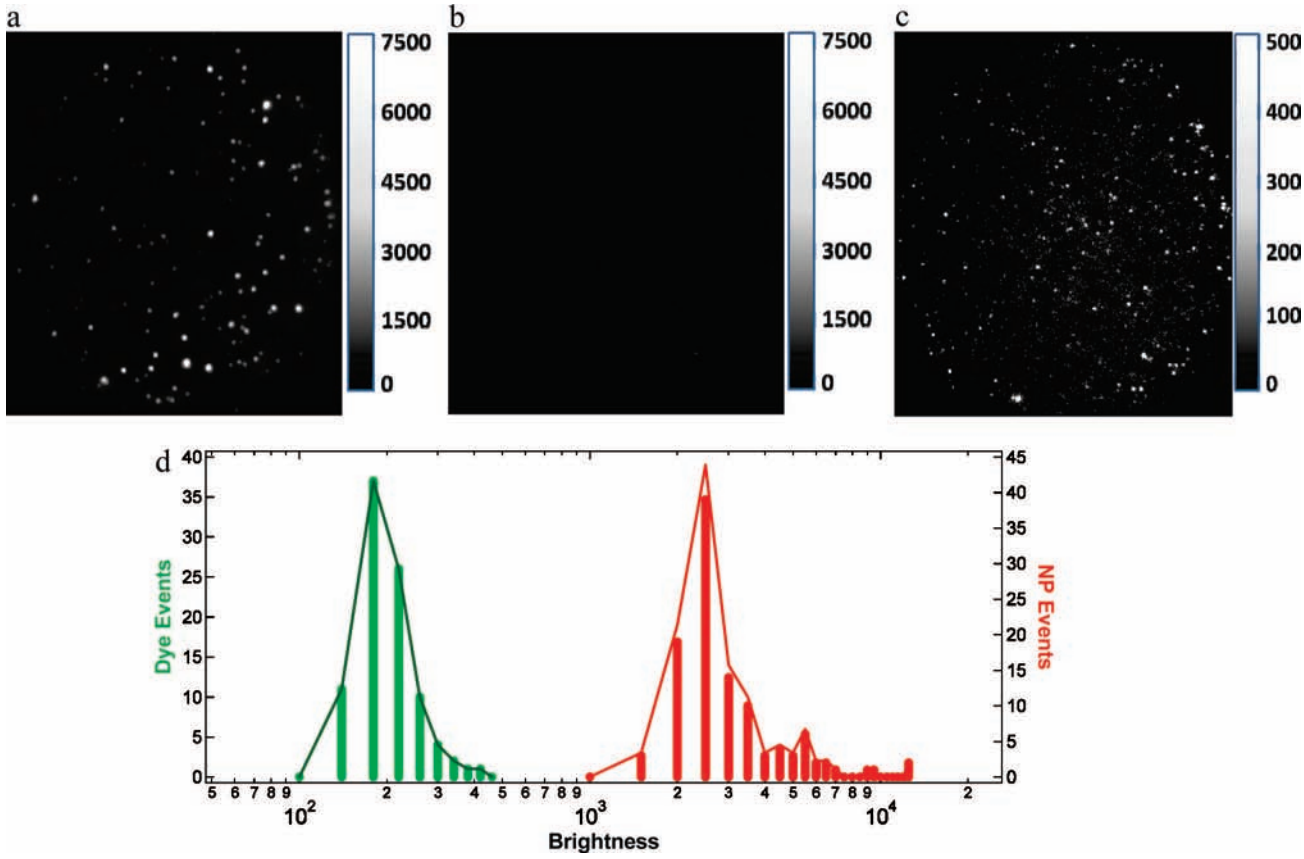

Figure 4. Imaging photoswitchable nanoparticles in their red fluorescence mode and fluorescein dye uses the same conditions, such as single-molecule fluorescence microscope setting and the excitation power. (a) The nanoparticle image scales from 0 to 7500 cps; (b) at such a scale, the fluorescein molecules are not visible. (c) To reveal the individual fluorescein molecules, panel c has been plotted at much lower scale, from 0 to 500 cps. Images a and b shares the same color scale, revealing the huge emission brightness intensity disparity between nanoparticles and organic dyes. (d) The histogram contrasts the measured nanoparticle brightness (red line and bars) with fluorescein (green line and bars). The nanoparticle most occurrence intensity is 38 times brighter than fluorescein dye after correction of the optimum excitation wavelength (a factor $\gamma = 2.7$).

optimum wavelength at 365 nm, the nanoparticles shine another ~2.7 times brighter. Therefore, when both fluorescein dye and the nanoparticle are excited at their respective optimum wavelengths, the nanoparticles fluoresce nearly 38 times brighter than the state-of-the-art organic dye fluorescein.

Copolymer Sequence and Composition Govern Nonspecific Interactions. To target disease tissue such as a tumor, the probe or the drug-delivery vehicle will need to be highly specific to the disease tissue and interact minimally with other surrounding normal tissue. The widely accepted synthetic materials that have little nonspecific interaction are poly(ethylene glycols) (PEG) because they seldom foul biological systems.[33,34] Here, we demonstrate that copolymer sequence and composition effectively control its nonspecific interactions with live cells. Adjusting the monomer ratio tunes the copolymer sequence and composition and affects its nonspecific interactions with live cells. To test nonspecific interactions, we incubated MSP-nanoparticles with either cancer or normal cells for 2 h in DMEM medium with 10% FBS (pH ≈ 7.4). After incubation, the medium was removed and cells were washed with PBS (pH = 7.2) three times to remove any residue-unbound nanoparticles. Cells were then imaged by use of 488- and 365-nm light to excite green and red channel images, respectively. Figure 5 displays the representative cell images.

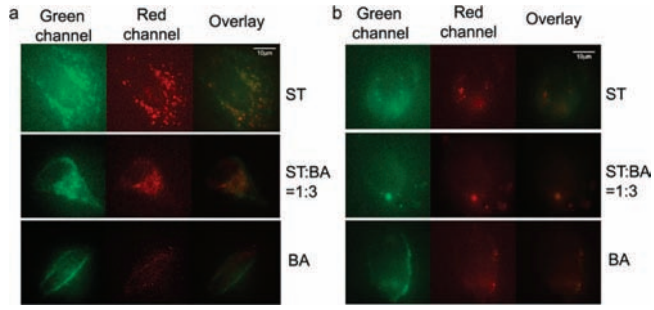

Figure 5. Live-cell imaging uses fluorescent color-switching nanoparticles. (a) Adjusting the monomer ST-to-BA ratio effectively reduces nonspecific interactions between nanoparticles and HeLa cells. The residue green fluorescence in the BA line is mostly due to cell autofluorescence. (b) Similar to panel a except that HeLa cells are replaced with noncancerous HEK-293 cells. In both panels, nanoparticles adhere to the cells only when the monomers A and BA are out of balance but undergo no endocytosis. The overlay images confirm the signals are from nanoparticles, not interference.

Tuning the monomer A:BA ratio imparts an obvious influence on how MSP-nanoparticles adhere to cancer cells (HeLa; Figure 5a), and to a less degree, normal cells (HEK-293; Figure 5b). Particularly, MSP-nanoparticles without BA *or* A monomer significantly bind to HeLa cell membranes, and their fluorescence brightens the cellular contour of HeLa cells. In sharp contrast, MSP-nanoparticles containing balanced A and BA comonomers hardly bind to HeLa cells (Table 1); fluorescence

(33) Leckband, D.; Sheth, S.; Halperin, A. J. *Biomater. Sci., Polym. Ed.* **1999**, *10*, 1125–1147.
(34) Lee, S.; Voros, J. *Langmuir* **2005**, *21*, 11957–11962.

Table 1. Copolymer Composition Tunes Nonspecific Interactions and Controls Endocytosis[a]

					nonspecific interactions[b]		endocytosis	
	single-particle brightness (au)	A (mmol)	ST (mmol)	BA (mmol)	HeLa cells (%)	HEK-293 cells (%)	HEK-293 cells	HeLa cells
1	432	0.56	1.00	0.00	100 ± 3	14 ± 1.5	no	no
2	426	0.56	0.25	0.75	28 ± 3	4 ± 1.5	no	no
3	412	0.56	0.00	1.00	5 ± 1.5	1 ± 1.5	no	no
4	438	0.00	0.25	0.75	70 ± 3	33 ± 3	yes	yes

[a] Additionally, all polymerization uses 30 g of water as solvent, 0.1 g of Tween 20 surfactant, and the following monomer: 0.2 mmol of acrylic acid (AA), 3 mg of MSP, 0.15 mmol of divinylbenzene (DVB), 0.02 mmol of 4,4′-azobis (4-cyanovaleric acid) (ABVA) initiator. [b] Cells were incubated with various nanoparticles for 1 h and then washed three times with PBS buffer (pH = 7.4). For each particle sample, more than 30 cells were imaged to analyze the nanoparticle adherence to a single cell line. Sample 1 has the strongest affinity to HeLa cells, and this total number of particles adhering to HeLa cells is normalized to 100%. Thus, the relative percentage of other nanoparticle samples is calculated to reveal each nanoparticle's affinity for the two cell lines.

microscopic imaging reveals that these cancer cell membranes are basically "free" from nanoparticles. This trend is also observed in normal HEK-293 cells. When either A or BA was absent, the nanoparticles adhered to the cells strongly. When the A:BA ratio reached a proper balance, nanoparticle adhesion to the cells almost disappeared. Interestingly, the copolymer nanoparticles can "distinguish" normal HEK-293 cells from HeLa cells. Nanoparticles having no BA monomer but high ST monomer prefer to bind HeLa cells much more than HEK-293 cells, yielding a 7:1 fluorescence intensity difference; nanoparticles having no A monomer also bind to HeLa cells more than HEK-293 cells in a 7:3 ratio. Therefore, the combination of A and BA monomers, not A or BA alone, significantly reduces nonspecific cell adhesion.

Optically Switchable Dual-Color Nanoparticles Enable High-Accuracy Cell Imaging. MSP-nanoparticles emit red fluorescence under 365-nm excitation and green fluorescence under 488-nm excitation. Consequently, the MSP-nanoparticles enable alternating red- and green-channel images. Therefore, only those features that emit both red and green fluorescence truly originate from the nanoparticle probes. The other emitters represent either interference or cell autofluorescence. The red and green channel overlay resulted in orange color in areas where the true nanoparticle probes reside and the single-color areas, regardless of red or green fluorescence, represent false positives.

To probe specific interactions, we selected nanoparticles that have a balanced A:BA ratio and thus little nonspecific interaction, and we decorated their surfaces with HMGA1 protein to provide specific interactions. Such modified nanoparticles bind to the HMGA1 receptor, which subsequently endocytoses the nanoparticle cargoes. Figure 6a reveals the time trajectories for HMGA1-modfied MSP nanoparticles. At 20 min, the nanoparticles mostly bind to the cell plasma membranes, illuminating the cellular contour. Endocytosis begins soon after; the brighter fluorescent spots light up cell organelles, and the early endosomes containing fluorescent cargoes emerge at 40 min. At later times, cells use motor proteins to actively transport nanoparticle-containing cargoes toward the perinuclear protoplasm, where the nanoparticles are stored in lysosomes. As more and more nanoparticles are sorted into the same cellular organelles such as late endosomes and lysosomes, the spotted fluorescence intensifies, illuminating the nuclear membrane area (Figure 6a, 60 min).

Because the fluorescence color of spiropyran dyes is quite tunable, we have not only green-to-red fluorescent nanoparticles but also blue-to-red fluorescent nanoparticles and even red color on−off fluorescent nanoparticles. Photoillumination switches all the fluorescence color. Figure 6b displays dual-color images of

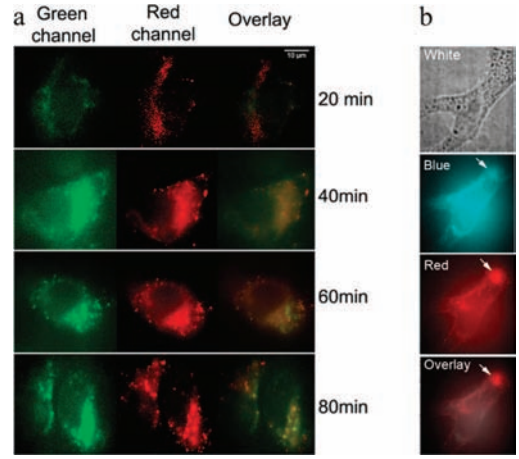

Figure 6. (a) Decorated with HMGA1a protein, MSP-nanoparticles undergo endocytosis as time elapses. Cells use motor proteins to collect these endocytosed cargoes into lysosomes and hence multiple confined nanoparticles manifest as brighter spots. (b) Functionalized by HMGA1a protein, MCSP-nanoparticles also bind to live cells and undergo endocytosis. The most intensive red-fluorescence spot (arrow) is unveiled to be a false positive because its signal cannot be corroborated in the blue channel.

the same cell on red and blue channels. Only those pixels in the images registering both blue and red fluorescence represent the true probe signals from MCSP-nanoparticles. Because cells are complex and alive, they synthesize new molecules constantly, including fluorescent molecules, and they also endocytose particles, including fluorescent particles. Now, dual-color nanoparticles can unambiguously distinguish nanoparticles from interfering emitters that fluoresce the same color. For example, the intensive red-fluorescence region indicated by an arrow (Figure 6b) has no blue counterpart, and therefore it must be from interfering cellular autofluorescence even though its intensity dominates the image.

The interactions between MSP-nanoparticles and live cells exemplify typical nonspecific interactions, and nanoparticles containing A monomer, at most, bind to the cell plasma membranes but undergo no endocytosis. Such nanoparticles undergo endocytosis only when functionalized with ligandlike molecules such as HMGA1a protein. Figure 7 and Table 1 demonstrate that nanoparticles without A monomer, however, induce nonspecific binding to cell membranes and amazingly trigger endocytosis. Although it is unclear how these negatively charged 120-nm nanoparticles cross the negatively charged cell membranes at pH $\approx$ 7.4, the experimental results divulge that monomer A plays a pivotal role in preventing polymer nanoparticles from being randomly endocytosed. Typically, most endocytosed nanoparticles are transported to late endosomes and lysosomes within 6 h and cease moving, but the nonspecific

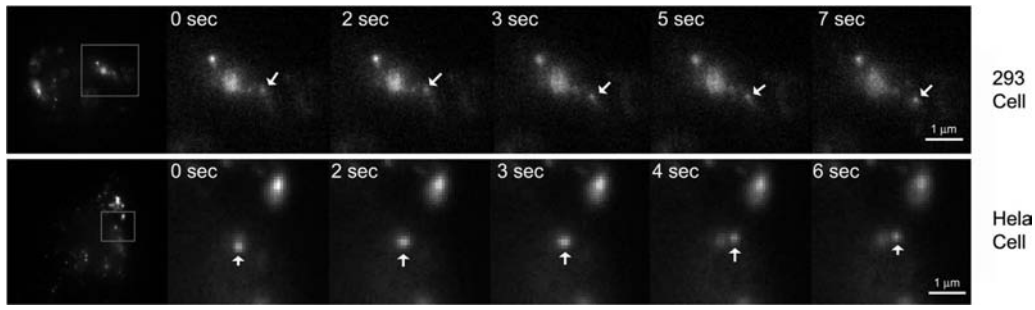

Figure 7. Interestingly, when acrylamide was removed from the nanoparticle formula, live cells (both HEK-293 and HeLa) readily endocytose the resulting MSP-nanoparticles. Such endocytosed cargoes (white arrow) remained in active transportation for at least 16 h. This phenomenon is very unusual because typical earlier endosomes would have matured into lysosomes at this time.

interaction-triggered endocytic cargoes are still actively moving even after 16 h from their entry. Why these endosomes containing nanoparticles without A monomer fail to mature into lysosomes remains a mystery, and one possible explanation resides with the surface-bound carboxyl groups. These carboxylate groups have a pK_a ~4 and continuously absorb protons as proteins pump protons into the endosomes, attempting to acidify the organelle. The nanoparticles perhaps function as a proton sponge and convert acidic protons into much less acidic weak acids, and this prevents the pH of early endosomes from lowering enough to mature into lysosomes.

Conclusions

To conclude, we have developed a novel class of organic dyes and such individual molecules can be photoswitched reversibly from red to green or blue fluorescence or even no fluorescence. These photoswitchable dyes enable much brighter nanoparticles whose fluorescence can also be switched accordingly. Previously, we have reported fluorescence color switching by a FRET mechanism within a single particle.[35] Now, no FRET is needed; one photoswitchable dye alternately emits two distinct colors. Photoswitchable probes not only provide high-accuracy cell imaging but also enable high-resolution microscopy such as PULSAR.[32] Currently, we are using these dyes and nanoparticles to demonstrate high-resolution microscopy beyond the diffraction limit.

Experimental Section

Synthesis and Characterization of Spiropyran Photoswitchable Dyes. Photoswitchable spiropyran derivatives were synthesized according to literature procedures;[36] their characterization data are summarized below.

3′,3′-Dimethyl-6-nitro-1′-(4-vinylbenzyl)spiro[chromene-2,2′-indoline] (SP). MALDI-TOF MS: $m/z = 425$ $[M + H]^+$; ^{1}H NMR (300 MHz, $CDCl_3$) $\delta = 1.30$ (3H, s), 1.34 (3H, s), 4.20 (1H, d, 17 Hz), 4.50 (1H, d, 17 Hz), 5.20 (1H, d, 10 Hz), 5.71 (1H, d, 17 Hz), 5.91 (1H, d, 10 Hz), 6.35 (1H, d, 8 Hz), 6.66 (1H, dd, 2 and 3 Hz), 6.72 (1H, m), 6.85−6.91 (2H, m), 7.04−7.14 (2H, m), 7.22−7.26 (2H, m), 7.33−7.35 (2H, m), 8.00−8.05 (2H, m).

5′-Methoxy-3′,3′-dimethyl-6-nitro-1′-(4-vinylbenzyl)spiro[chromene-2,2′-indoline] (MSP). MALDI-TOF MS: $m/z = 455$ $[M + H]^+$; ^{1}H NMR (300 MHz, $CDCl_3$) $\delta = 1.31$ (3H, s), 1.32 (3H, s), 3.76 (3H, s), 4.11 (1H, d, 17 Hz), 4.44 (1H, d, 17 Hz), 5.22 (1H, d, 10 Hz), 5.72 (1H, d, 17 Hz), 5.91 (1H, d, 10 Hz), 6.22 (1H, d, 8 Hz), 6.59 (1H, dd, 2 and 3 Hz), 6.68 (1H, m), 6.75 (1H, d, 2 Hz), 6.78−6.88 (2H, m), 7.23 (1H, d, 3 Hz), 7.33−7.36 (2H, m), 7.98 (1H, d, 3 Hz), 8.02−8.05 (2H, m).

5′-Methoxy-3′,3′-dimethyl-6-cyano-1′-(4-vinylbenzyl)spiro[chromene-2,2′-indoline] (MCSP). MALDI-TOF MS: $m/z = 435$ $[M + H]^+$; ^{1}H NMR (300 MHz, $CDCl_3$) $\delta = 1.29$ (3H, s), 1.31 (3H, s), 3.76 (3H, s), 4.09 (1H, d, 17 Hz), 4.43 (1H, d, 17 Hz), 5.22 (1H, d, 10 Hz), 5.72 (1H, d, 17 Hz), 5.87 (1H, d, 10 Hz), 6.20 (1H, d, 8 Hz), 6.56 (1H, dd, 2 and 3 Hz), 6.64 (1H, m), 6.69 (1H, d, 2 Hz), 6.74−6.80 (2H, m), 7.22 (1H, m), 7.25 (2H, m), 7.36−7.38 (2H, m), 7.40 (1H,d, 2 Hz).

3′,3′-Dimethyl-6-cyano-1′-(4-vinylbenzyl)spiro[chromene-2,2′-indoline] (CSP). MALDI-TOF MS: $m/z = 405$ $[M + H]^+$; ^{1}H NMR (300 MHz, $CDCl_3$) $\delta = 1.29$ (3H, s), 1.33 (3H, s), 4.18 (1H, d, 17 Hz), 4.48 (1H, d, 17 Hz), 5.22 (1H, d, 10 Hz), 5.72 (1H, d, 17 Hz), 5.86 (1H, d, 10 Hz), 6.33 (1H, d, 8 Hz), 6.66 (1H, dd, 2 and 3 Hz), 6.75 (1H, m), 6.78−6.90 (2H, m), 7.04−7.13 (2H, m), 7.22−7.25 (2H, m), 7.33−7.40 (4H, m).

Synthesis and Characterization of Nanoparticles with Embedded Spiropyran Dyes. Reagents. All reagents and solvents were purchased from Aldrich Chemical Co. and used as received except when stated otherwise. Acrylamide (A) and 4,4′-azobis-(4-cyanovaleric acid) (ABVA) was recrystallized before use. Styrene (ST, 99%), acrylic acid (AA), and butyl acrylate (BA) were distilled under reduced pressure.

Emulsion Polymerization. Emulsion polymerization was carried out according to the literature procedure as reported elsewhere.[28−30] UV analysis of the organic phase ($CHCl_3$) extracted from the emulsion mixture suggests that more than 95% of the initial spiropyran comonomer was incorporated into the final nanoparticles. The as-synthesized nanoparticles showed no obvious aggregation as measured by dynamic light scattering.

Characterization. ^{1}H NMR spectra were recorded in $CDCl_3$ on a JEOL JNM-AL300 instrument. Dynamic light scattering (DLS) measurements were carried out on a Beckman-Coulter N4 instrument at fixed scattering angles of 62.6° and 90° with the 632.8 line of a He−Ne laser as the excitation source; standard polystyrene microspheres were used to calibrate the instrument. The average particle sizes and size distributions were obtained from the autocorrelation decay functions by CONTIN analysis with a standard software package supplied by Beckman-Coulter. A JEOL 1010 transmission electron microscope (TEM) operated at 100 kV was employed to obtain TEM images. The microscope sample was prepared by placing a drop of the polymer dispersion on a carbon-coated Cu grid, followed by solvent evaporation at room temperature.

Sample Preparation for Microscopy. Cover glasses (Gold Seal no. 1, Fisher) were cleaned by a protocol comprising sonication in 2% Micro 90 for 30 min, rinsing thoroughly with 18 MΩ water, drying in an oven, soaking in Chromerge for 1 h, rinsing thoroughly with 18 MΩ water, and finally heating gently in a methane flame to dryness. After being cooled slowly, the cover glasses were stored in a dust-free container. Nanoparticle samples were prepared by spin-coating (4000 rpm) ~30 μL of a dilute suspension of nanoparticles in spectroscopic-grade ethanol onto

(35) Zhu, L. Y.; Wu, W. W.; Zhu, M. Q.; Han, J. J.; Hurst, J. K.; Li, A. D. Q. *J. Am. Chem. Soc.* **2007**, *129*, 3524–3526.
(36) Tomasulo, M.; Kaanumal, S. L.; Sortino, S.; Raymo, F. M. *J. Org. Chem.* **2007**, *72*, 595–605.

a cover glass. Samples were diluted sequentially until the density of nanoparticles on the cover glass was suitable for single-particle measurements. For cell samples, the glass-bottom 35-mm MatTek's culture dishes (MatTek Corp.) were filled with a DMEM solution. Washed cells were transferred into the well and allowed to settle before inspection.

Microscope Design. Samples were placed on a custom-built stage of an inverted microscope (Zeiss Axiovert 200) equipped with a high numerical aperture oil immersion objective (Zeiss, 100×, 1.3 NA) and an $x-y$ nanopositioner stage (Mad City Laboratories). Connected to the side port of the microscope was a spectrometer (Acton Research Corp.) coupled to a liquid nitrogen-cooled charge-coupled device (CCD) detector (Princeton Instruments, Roper Scientific). The spectrometer was equipped with both a mirror for imaging and a grating for spectroscopy. An avalanche photodiode (APD) was used to collect photons from the bottom microscope port. Excitation entering the back port of the microscope was redirected by an appropriate filter set into the back aperture of the objective. Emission light was collected through the same objective and directed to the side or bottom port of the microscope.

Cell Growth. Transformed human embryonic kidney (HEK-293) cells were grown in 24-well culture plates until cell populations reached ~105 cells/well. A 1 pmol nanoparticle suspension was prepared in 50 μL of DMEM (Dulbecco's modified Eagle medium). Mammalian cells were incubated for 5 min at room temperature, after which the dilute nanoparticle suspension was added, followed by an additional 20-min incubation at room temperature.

Delivery of Nanoparticles into Living Cells. Nanoparticles were delivered into cells by adding 100 μL of the nanoparticle suspension to each cell-containing well in the culture plate. After incubation for 5 h at 37 °C in a CO_2 incubator, the cells were washed with 500 μL of DMEM and resuspended in 500 μL of DMEM containing 10% FBS (fetal bovine serum).

Wide-Field Nanoparticle Imaging. For wide-field imaging of nanoparticles, a mercury vapor short-arc lamp illuminator (Zeiss HBO 100) was mounted to the back illumination port of the microscope. Two filter sets, each consisting of an excitation filter (ex), dichroic beam splitter (bs), and emission filter (em), were used to isolate either the 365-nm (Zeiss, filter set 2; ex 365, bs 295, em 420) or the 488-nm (Zeiss, filter set 16; ex 485/20; bs 510; em 515) excitation lines from the mercury lamp spectrum. Excitation light was not attenuated. Samples were first illuminated with 365-nm light to convert the photoswitches to their red-fluorescence mero-forms, thereby facilitating focusing of the nanoparticles via CCD imaging. After achieving focus, the 365-nm light was blocked and a new area on the cover glass was moved into the illumination area via the nanopositioner. The new area was illuminated with 365-nm light for 3−4 s to photoswitch spiropyran into fluorescent merocyanine. Next, nanoparticle image acquisition was carried out with 488-nm illumination. Red fluorescence was obtained via a red long-pass filter (620 nm) and a CCD detector. All images were collected with a 3-s integration time in WinSpec/32 software. Two-dimensional black and white CCD images were converted into 3-D color surface plots in Igor Pro software (Wavemetrics).

Cell Imaging. For cell imaging, an argon ion laser (488 nm) and hand-held UV lamp were used instead of the mercury lamp because of its heating effects. Cells were first photographed under white light illumination. For MSP-nanoparticle live cell imaging, the red fluorescence channel was obtained via a red long-pass filter (620 nm) and a 365-nm pulse to photoswitch on merocyanine followed by 488-nm fluorescence excitation, whereas the green fluorescence channel was acquired via 488-nm excitation and a bandpass filter (510 ± 40 nm). For MCSP-nanoparticle live cell imaging, the red fluorescence channel was obtained via a red long-pass filter (620 nm) and a 300-nm pulse to photoswitch on merocyanine followed by 488-nm fluorescence excitation, whereas the blue fluorescence channel was acquired via 365-nm excitation and a long-pass filter (420 nm) because 365-nm excitation cannot photoswitch on red fluorescence.

Acknowledgment. We acknowledge the support of National Institute of General Medical Sciences (GM065306) and National Science Foundation (CHE-0805547).

JA805150G